Experimental results from high energy proton-nucleus interactions, critical phenomena, and the thermal liquid drop model of fragment production

A. S. Hirsch, A. Bujak, J. E. Finn,* L. J. Gutay, R. W. Minich,†
N. T. Porile, R. P. Scharenberg, and B. C. Stringfellow
Department of Physics and Department of Chemistry, Purdue University, West Lafayette, Indiana 47907

F. Turkot
Fermi National Accelerator Laboratory, Batavia, Illinois 60510
(Received 22 August 1983)

In an inclusive experiment, isotopically resolved fragments, $3 \leq Z \leq 13$, produced in high-energy proton-nucleus collisions have been studied using a low mass time-of-flight, gas ΔE-silicon E spectrometer and an internal gas jet. Measurement of the kinetic energy spectra from 5 to 100 MeV enabled an accurate determination of fragment cross sections from both xenon and krypton targets. Fragment spectra showed no significant dependence on beam energy for protons between 80 and 350 GeV/c. The observed isobaric yield is given by $Y \alpha A_f^{-\tau}$, where $\tau \sim 2.6$ for both targets; this also holds for correlated fragment data. The power law is the signature for the fragment formation mechanism. We treat the formation of fragments as a liquid-gas transition at the critical point. The critical temperature T_c can be determined from the fragment isotopic yields, provided one can set an energy scale for the fragment free energy. The high energy tails of the kinetic energy spectra provide evidence that the fragments originate from a common remnant system somewhat lighter than the target which disassembles simultaneously via Coulomb repulsion into a multibody final state. Fragment Coulomb energies are about $\frac{1}{10}$ of the tangent sphere values. The remnant is characterized by a parameter T, obtained from the high energy tails of the kinetic energy distributions. T is interpreted as reflecting the Fermi momentum of a nucleon in this system. Since $T \gg T_c$, and T is approximately that value expected for a cold nucleus, we conclude that the kinetic energy spectra are dominated by this nonthermal contribution.

[NUCLEAR REACTIONS Xe(p,X), Kr(p,X), $80 \leq E_p \leq 350$ GeV; measured $\sigma(E,\theta)$, X = Li to Al, $\theta = 34°$. Fragmentation.]

I. INTRODUCTION

The production of nuclear fragments in reactions between nucleons and heavy nuclei, as well as between heavy ions, has been known for three decades.[1] Emulsion[2] and radiochemical[3] studies have been particularly well suited for investigating some of the features of these reaction products, which typically are less than about one third of the original target mass. In particular, it has been clearly established that fragmentation is a high energy process, characterized by a threshold of about 1 GeV for incident protons, and a high charged particle multiplicity indicative of a central collision. The question of the fragment production mechanism has had to wait for two important technical developments: high energy, high intensity beams in order to achieve the statistics necessary for a detailed study of fragment systematics, and detectors capable of high resolution measurements for fragments over a wide range of both charge and kinetic energy. The success of experiments at lower incident proton energies has shown convincingly that counter experiments can make a detailed and comprehensive examination of these nuclear fragments.[4,5] More recently, use of an internal gas target and the circulating proton beam at Fermilab has permitted the extension of counter techniques to energies as high as 400 GeV.[6]

In two previous Letters we have noted that the data display features which are consistent with the interpretation of fragment production as a critical phenomenon.[7,8] In our first paper[7] we noted that the inclusive fragment mass yield from both krypton and xenon targets obeys a power law,

$$\text{yield}(A_f) \propto A_f^{-\tau}, \quad \tau \sim 2.6, \tag{1}$$

where A_f is the fragment mass number. Thus, τ is independent of target mass for heavy targets. It is well known that real gases, near the critical point, exhibit cluster distributions which obey a power law with an exponent between 2.1 and 2.3.[9] On very general theoretical grounds τ is expected to lie between 2 and 3.[10] In our second paper,[8] we adapted the Fisher droplet model,[10] which describes the liquid-gas phase transition for a single component system, to a two component system composed of neutrons and protons. We will hereafter refer to this description as the thermal liquid drop model (TLDM) of fragment production. In this paper we present the results of our analysis of the fragment kinetic energy spectra. We conclude that they can be understood in a manner which

is consistent with the TLDM model. A necessary condition for the success of this model is that it can predict the general features of the mass yields, the isotopic yields, and the kinetic energy spectra. Such a phenomenological model should describe the data with a minimum number of free parameters.

The experiment was performed at the Internal Target Area of the Fermi National Accelerator Laboratory (FNAL), and thus enabled, during the accelerator cycle, a study of the energy dependence of the fragment production cross section between 80 and 350 GeV/c incident proton momentum. Since we used the full accelerator beam in a parasitic mode, we were able to obtain the necessary high statistics data (10^8 events). It is important to measure as much of the fragments's kinetic energy spectra as possible in order to make an accurate determination of the fragment yields. Thus, in addition to the 15 ng/cm^2 gas jet target, it was crucial to design a spectrometer which presented a minimal mass (150 μg/cm^2) to the fragments in their traversal of the apparatus. The charge determination was accomplished by the standard differential (ΔE) and total energy (E) measurement. To extend our measurement to the lowest possible kinetic energy, a gas ionization detector was used to measure ΔE. The combination of a time-of-flight (TOF) and ΔE-E system enabled fragment identification over a wide range of fragment mass, charge, and kinetic energy.

Experimental details of this high energy experiment, in which the properties of isotopically resolved fragments of charge $2 \leq Z \leq 13$ produced from xenon and krypton targets were measured, are discussed in Sec. II. Results are presented in Sec. III, followed by a discussion in Sec. IV. Our major conclusions are summarized in Sec. V.

II. DESCRIPTION OF THE EXPERIMENTAL APPARATUS

A. General

Experiments attempting to detect heavy nuclear fragments with kinetic energies of less than 1 MeV/nucleon are necessarily restricted to using thin targets, thus sacrificing the counting rate attainable with thicker targets. The gas jet target (see Fig. 1) located in the main ring at FNAL was ideally suited for studying nuclear fragments, since with each cycle of the accelerator about 2×10^{13} protons traverse the target at a rate of 47 kHz. Target thicknesses of about 15 ng/cm^2 resulted in counting rates higher than those attainable on external beam lines with reasonably thick (< 10 μg/cm^2) foil targets.

The mixed gas targets used during the course of the experiment are listed in Table I. The hydrogen component was used in order to normalize our data by detecting in a monitor telescope elastically scattered recoil protons at a laboratory angle of about 85°. The thicknesses for various mixed gases are listed in Table I.

Two fragment telescopes were located at 34° and 76° with respect to the beam direction. The former, hereafter referred to as $T2$, was designed to detect heavy slow fragments, and was terminated by a hybrid gas-silicon detector. The latter, $T4$, was limited to the detection of lighter,

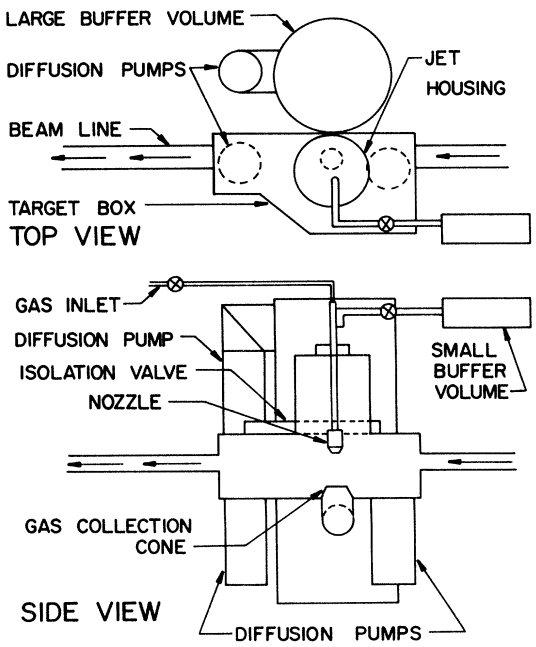

FIG. 1. Schematic of the gas jet target at the Internal Target Area, Fermilab.

faster fragments than $T2$. The two telescopes were identical except for the terminating detectors.

The forward angle telescope, $T2$, consisted of three units of time-of-flight detectors followed by a gas ionization chamber, which was terminated by a silicon heavy ion detector. The apparatus is shown schematically in Fig. 2. Each TOF unit utilized microchannel plate (MCP) devices which act as electron multipliers.[11] The TOF measurement was made with one "START" and two different "STOP's." Since the TOF detectors required a vacuum of less than 5×10^{-5} Torr to ensure their long-term operation, they were housed in aluminum boxes which could be vacuum isolated from the rest of the system.

The hybrid gas detector was based on a design by Fowler and Jared[12] but was modified to accommodate a larger entrance window and a larger silicon detector. An unsupported 1.9 cm diameter stretched polypropylene window[13] 80 mg/cm^2 thick served to separate the high vacuum (10^{-6} Torr) in the channel plate (CP) boxes from the interior of the gas detector at 20 Torr. The apparatus and its associated electronics are described in greater detail in Ref. 14.

The 76° telescope shown in Fig. 3, $T4$, was designed for fragment identification for charges $2 \leq Z \leq 8$. This was

TABLE I. Target gas mixtures and noble gas thicknesses.

Mixture (% partial pressure)	Thickness (ng/cm^2)
10% Xe—90% H_2	21
20% Kr—80% H_2	26
10% Kr—90% H_2	13

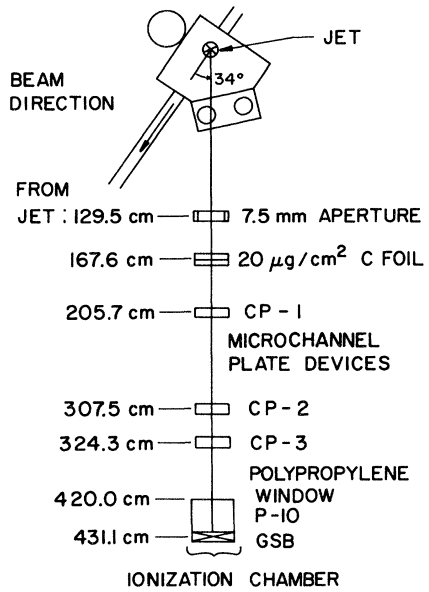

FIG. 2. Schematic of the heavy fragment telescope, $T2$, located at 34° laboratory scattering angle.

accomplished using a double ΔE, E, Veto series of silicon surface barrier detectors, whose characteristics are given in Table II. For the heaviest and slowest fragments in the above range, the second ΔE detector served as an E, and the E as a Veto. The TOF detectors for $T4$ were identical in design and configuration to those in $T2$. The stability of the system was monitored by a pulser signal, whose rate was derived from the counting rate, and by radioactive alpha sources on each silicon detector.

The data acquisition program was a modified version of the SNAP program developed at Argonne National Laboratory.[15] Event information was written onto magnetic tape for later off-line analysis.

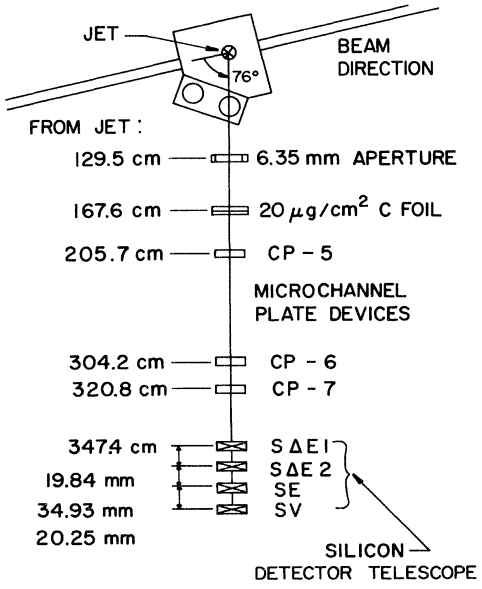

FIG. 3. Schematic of the light fragment telescope, $T4$, located at 76° laboratory scattering angle.

TABLE II. Silicon surface barrier detector specifications.

Telescope	Detector	Thickness (μm)	Area (mm^2)
Monitor	ΔE	50	50
	E	2000	50
	Veto	1013	50
$T2$	GSB	60	300
$T4$	$\Delta E1$	19.3	100
	$\Delta E2$	19.2	100
	E	498	100
	Veto	1500	100

The analysis was done on a VAX 780 computer at the Purdue High Energy Physics computing facility. The events on each raw data tape were identified according to telescope and written onto a tape containing only telescope specific events. At this time, pulser events were counted and dead times computed. Each event on these telescope tapes was then identified by charge. Corrections for energy losses, which are strongly charge dependent, were made at this time. Masses were then computed and tapes containing kinetic energy spectra for each mass were generat-

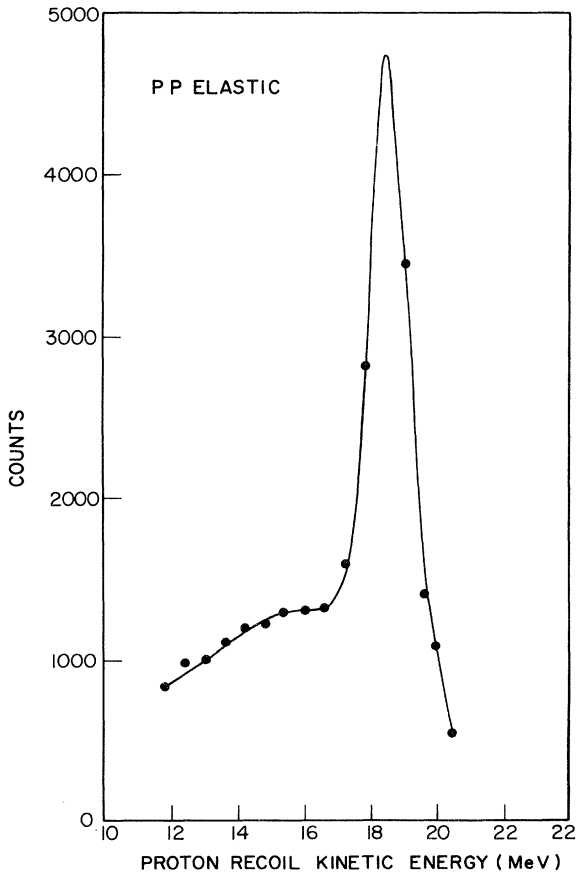

FIG. 4. Proton spectrum observed by the monitor telescope at about 85° in the laboratory. Normalization has been achieved by fitting to the p-p elastic peak. The solid curve represents the fit.

ed. Below we discuss some of the particular details for each telescope.

B. Data reduction of events detected by the monitor telescope

The monitor telescope could detect protons with kinetic energies between approximately 7 and 21 MeV, deuterons between 10 and 29 MeV, and tritons between 15 and 33 MeV. The proton spectrum consisted of a clearly identifiable peak at about 18 MeV superimposed on a slowly varying background. The peak arose from elastic scattering of protons in the hydrogen component of the gas jet into the detector located at 85°. The background is owing to scattering from both the hydrogen and heavy gas component in the target (Fig. 4). The protons, deuterons, and tritons were separated from one another by plotting ΔE vs E_{total} for all events. It could be seen from such a plot that there were three distinct bands of events and that the bands had a similar curvature. Thus one functional form of the type $\Delta E = F(E_{\text{total}})$ could be used to straighten the bands for all species. After splitting off the different species, we could perform fits to the proton kinetic energy spectrum. The form used was a Gaussian plus a background composed of a constant, linear, and quadratic contribution. Chi-square for the fits to the proton spectrum were about 1.5 per degree of freedom.

The resulting fits to the p-p elastic peak were used to determine absolute cross sections for fragment production. The geometry of the monitor was known, as was the energy dependence of the p-p elastic cross section between 80 and 350 GeV/c, the range of interest here. The p-p cross section is slowly varying over this range, and so the median value of $(d\sigma/d\Omega)(\text{pp}) = 5.88$ mb/sr was used.[16]

The monitor was useful in verifying that the hydrogen and heavy gas components did not separate significantly as a function of transverse distance from the central axis of the gas jet. By measuring the ratio (deuterons + tritons)/elastic as a function of distance from the jet axis, we confirmed that to within 10%, the ratio of hydrogen to heavy gas in the jet was a constant and equal to the ratio of partial pressures in the gas bottle.

The p-p elastic area was divided by the average beam intensity and this quantity was examined for significant variations on a run-by-run basis. No unexplainable variation occurred.

C. Data reduction of events detected by the heavy fragment telescope ($T2$)

The gas detector, filled with P-10 gas at 20 Torr, was able to detect fragments from charge 2–14. The alpha particle kinetic energy spectrum, however, was restricted to energies less than 13 MeV, and thus was not used. Charges 3–13 were easily separated by expanding a plot of ΔE vs the total kinetic energy, E_T. A typical unexpanded plot is shown in Fig. 5. At every value of E_T, the range of ΔE as a function of charge was determined by examining these scatter plots. These values were put into a look-up table. Each event was then labeled by an integer

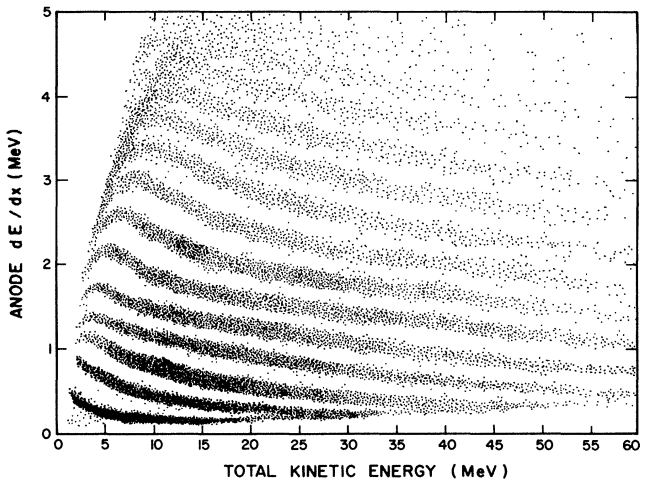

FIG. 5. A typical ΔE vs E_t plot as measured by the gas detector ($T2$) from p-Xe collisions.

value of charge according to its measured value of ΔE, and the entire event, now with a charge identifier, was written onto another tape. Corrections for energy losses suffered by a fragment as it traversed the telescope and for pulse height defect in the silicon detector were made at this time. The energy loss corrections were crucial in obtaining our optimum mass resolution, about 1.5% for the aluminum isotopes, as shown in Fig. 6. These corrections were small in magnitude (less than 5 MeV), but were not insignificant at low energies.

A correction was also made to account for the increase in time-of-flight between the CP START and the surface barrier STOP as the fragment lost energy in the gas detector. A charge and energy dependent correction was applied to account for events lost owing to channel plate

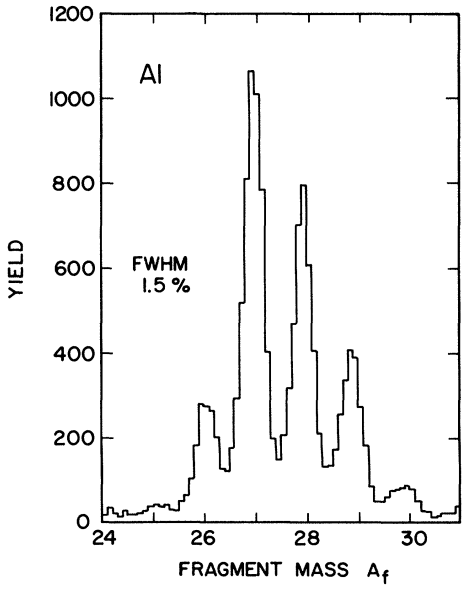

FIG. 6. Aluminum masses as measured by $T2$ and corrected as discussed in the text.

inefficiency. The channel plate efficiencies were determined from the data themselves by using the information recorded for each event. If an event was recorded, it necessarily had both a ΔE and an E signal and traversed all three MCP detectors. The efficiency of each MCP detector was then calculated for each Z in steps of 1 MeV over the range of the fragment spectrum by noting which TOF signals were present and which were not. For fragments heavier than carbon, the MCP detectors were nearly 100% efficient. Our channel plate corrections are in good agreement with estimates based on fundamental principles of channel plate operation.[17]

Finally, a correction was made for events lost owing to multiple scattering in our system. A Monte Carlo computer program was developed to calculate the multiple scattering of fragments through our spectrometer. The essential physical parameter, the projected half-angle of the distribution, was calculated based on the work of Meyer.[18] He specifically addressed the case of multiply-charged particles traversing thin foils. We checked our calculation by simulating the experimental conditions as described by Eastham.[19] We obtained excellent agreement with the results reported in Ref. 19. The isotopic dependence of this correction was ignored. The correction for a 1 MeV/nucleon carbon fragment was about 3%.

D. Data reduction for events detected by the light particle telescope ($T4$)

The data from $T4$ were analyzed in much the same manner as those from $T2$, the only major difference being the two classes of events, those which fired both ΔE's and stopped in the E detector, and those which stopped in the second ΔE detector. This telescope detected fragments with $2 \leq Z \leq 8$. Only the results from the alpha particles have been used in the analysis presented in this paper. Corrections similar to those made for $T2$ were made. Time of flight was measured over the two MCP flight paths, and, in addition, between MCP 1 and the second ΔE detector.

III. EXPERIMENTAL RESULTS

We now discuss the results of our analysis of the data from $T2$ with the inclusion of the alpha particles from $T4$. A previous experiment[6] found no evidence for beam energy dependence of fragment production between 30 and 350 GeV/c proton momentum. The present experiment enabled another look for such an effect with the advantage of individual isotopic resolution for masses 6–31. Beryllium, carbon, and oxygen kinetic energy spectra were examined in 25 GeV/c momentum bins, and no statistically significant evidence for a beam momentum dependence was found between 80 and 350 GeV/c. Therefore, the data were summed over all beam energies.

The data were normalized using the ratio of measured fragment yield to the measured p-p elastic scattering yield. Absolute target thicknesses were determined from profile studies of the gas jet performed using the proton beam, and are listed in Table I.

Absolute cross sections were obtained by first calculating the absolute ^{12}C cross section for 10 out of a total of 50 runs. These run-by-run cross sections were then averaged to give a final absolute ^{12}C cross section. The absolute cross section of another fragment was obtained according to the equation

$$\frac{d\sigma}{d\Omega}(Z_f,A_f)=\frac{\text{corrected yield } (Z_f,A_f)}{\text{corrected yield } ^{12}\text{C}}\frac{d\sigma}{d\Omega}(^{12}\text{C}) . \quad (2)$$

The error associated with each fragment's total cross section is the sum of the statistical error associated with that fragment's yield and the error in the determination of the absolute cross section of ^{12}C added in quadrature. Absolute cross sections and errors are listed in Tables III and IV. We estimate a systematic error of about 15%.

A. Fragment mass yields

The simplest way to represent the data is to sum the yield of all fragment species at a given fragment mass number A_f. The measured fragment yield must be corrected for fragments lost because of experimental hardware and software cutoffs. These corrections were first made by extrapolating by eye the kinetic energy spectra at low energy to zero and the high energy exponential tail to infinity. Later, after the kinetic energy spectra had been fit using a functional form motivated by the droplet model (discussed in Sec. III C), the fitted yields were compared to those first obtained. The two methods agreed to within 2%. The percentage of the yield extrapolated was as large as 40% for the heaviest fragments, and averaged about 10% for all fragments. Several kinetic energy spectra are shown in Fig. 7. All corrections have been applied to the spectra.

In Fig. 8 we have plotted the fragment yield from the xenon and krypton targets as a function of fragment mass, A_f. Since our fragment telescopes were not designed to detect fragments lighter than helium, it was necessary to examine data from other experiments for information on the lighter fragment species. In particular, emulsions[20] bombarded by protons above 5 GeV indicate that on the average 18–20 protons are associated with each ^{8}Li fragment. A ^{8}Li fragment is easily identified in an emulsion by its characteristic "hammer track" decay. The data also indicate that when 20 protons are observed, the probability for observing a ^{8}Li is between 5 and 10 percent. The implication is that fragments other than ^{8}Li are present the remaining 90–95 % of the time. Although there are considerable uncertainties in the determination of the above percentages in the emulsion data, we can use this information to approximate the yield of neutrons and protons which were produced in association with the fragments. It should be noted, therefore, that mass $=1$ is being treated differently than the heavier masses in that the latter were measured inclusively. Protons and neutrons, however, can result from interactions which do not involve the fragmentation mechanism, and these should be excluded from our consideration. Our own data indicate that ^{8}Li is approximately 5% of the fragment yield. If we

TABLE III. Normalized differential cross sections for fragments produced from xenon. Only statistical errors have been included.

Z	A	$d\sigma/d\Omega$ (mb/sr)	Error (%)	Z	A	$d\sigma/d\Omega$ (mb/sr)	Error (%)
3	6	2.76	6.6	9	20	0.378	6.6
3	7	6.89	6.6	9	21	0.213	6.6
3	8	2.02	6.6	9	22	0.0456	6.8
3	9	0.587	6.6	9	23	0.0116	7.4
4	7	1.65	6.6	9	24	0.00119	12.5
4	9	2.99	6.6	10	19	0.0195	7.1
4	10	2.91	6.6	10	20	0.154	6.6
4	11	0.292	6.6	10	21	0.319	6.6
4	12	0.0884	6.7	10	22	0.368	6.6
5	10	1.54	6.6	10	23	0.129	6.6
5	11	4.89	6.6	10	24	0.0475	6.8
5	12	1.24	6.6	10	25	0.00636	8.0
5	13	0.452	6.6	11	21	0.0124	7.3
5	14	0.0299	6.9	11	22	0.0839	6.7
5	15	0.00938	7.6	11	23	0.294	6.6
6	11	0.447	6.6	11	24	0.226	6.6
6	12	2.02	6.6	11	25	0.149	6.6
6	13	2.21	6.6	11	26	0.0400	6.8
6	14	1.23	6.6	11	27	0.0115	7.4
6	15	0.190	6.6	11	28	0.00186	10.7
6	16	0.0644	6.7	12	23	0.0122	7.3
6	17	0.00614	8.0	12	24	0.103	6.6
7	13	0.0776	6.7	12	25	0.192	6.6
7	14	0.656	6.6	12	26	0.242	6.6
7	15	1.94	6.6	12	27	0.104	6.6
7	16	0.436	6.6	12	28	0.0455	6.8
7	17	0.259	6.6	12	29	0.00891	7.6
7	18	0.0516	6.7	13	25	0.00708	7.9
7	19	0.0138	7.3	13	26	0.0396	6.8
7	20	0.00137	11.9	13	27	0.164	6.6
8	15	0.0873	6.7	13	28	0.150	6.6
8	16	0.741	6.6	13	29	0.114	6.6
8	17	0.526	6.6	13	30	0.0400	6.8
8	18	0.527	6.6	13	31	0.0156	7.2
8	19	0.161	6.6	14	28	0.0558	6.7
8	20	0.0555	6.7	14	29	0.107	6.6
8	21	0.00773	7.8	14	30	0.170	6.6
9	17	0.0276	6.9	14	31	0.144	6.6
9	18	0.144	6.6	14	32	0.139	6.6
9	19	0.390	6.6	14	33	0.134	6.6

TABLE IV. Ratio of the free energy parameters to temperature as determined by the fits to the isotopic yields.

Parameter	Xe	Kr
Volume βa_v	4.30	4.35
Surface βa_s	1.63	2.04
Coulomb βa_C	0.149	0.124
Symmetry βa_a	6.91	7.19
Pairing βa_p	1.80	1.63
Proton chemical potential $\beta\mu_p$	−3.45	−3.40
Neutron chemical potential $\beta\mu_n$	−2.31	−2.35
Power law exponent τ (fixed)	2.64	2.65

then assume that for every fragment there are about 19 protons and $1.3\times 19=25$ neutrons, accounting for the n/p ratio in the remnant mass region, we arrive at an estimate for the yield of mass = 1.

We also noted that unlike the mass = 1 point which is correlated to fragment (^{8}Li) emission, the mass =4 point is inclusive. It was obtained from the data acquired by $T4$, assuming approximate isotropy. Certainly alphas are produced by many mechanisms, not just by fragmentation. It is unlikely that we have overestimated the yield at mass 4 attributable to the fragmentation process. However, in the spirit of the TLDM model, we feel justified in treating ^{4}He on an equal footing with the other composite fragment data. A recent experiment by Warwick *et al.*[21] has shown that fragment multiplicities and cross sections for fragments in the range $2\leq Z_f\leq 12$ are essentially the

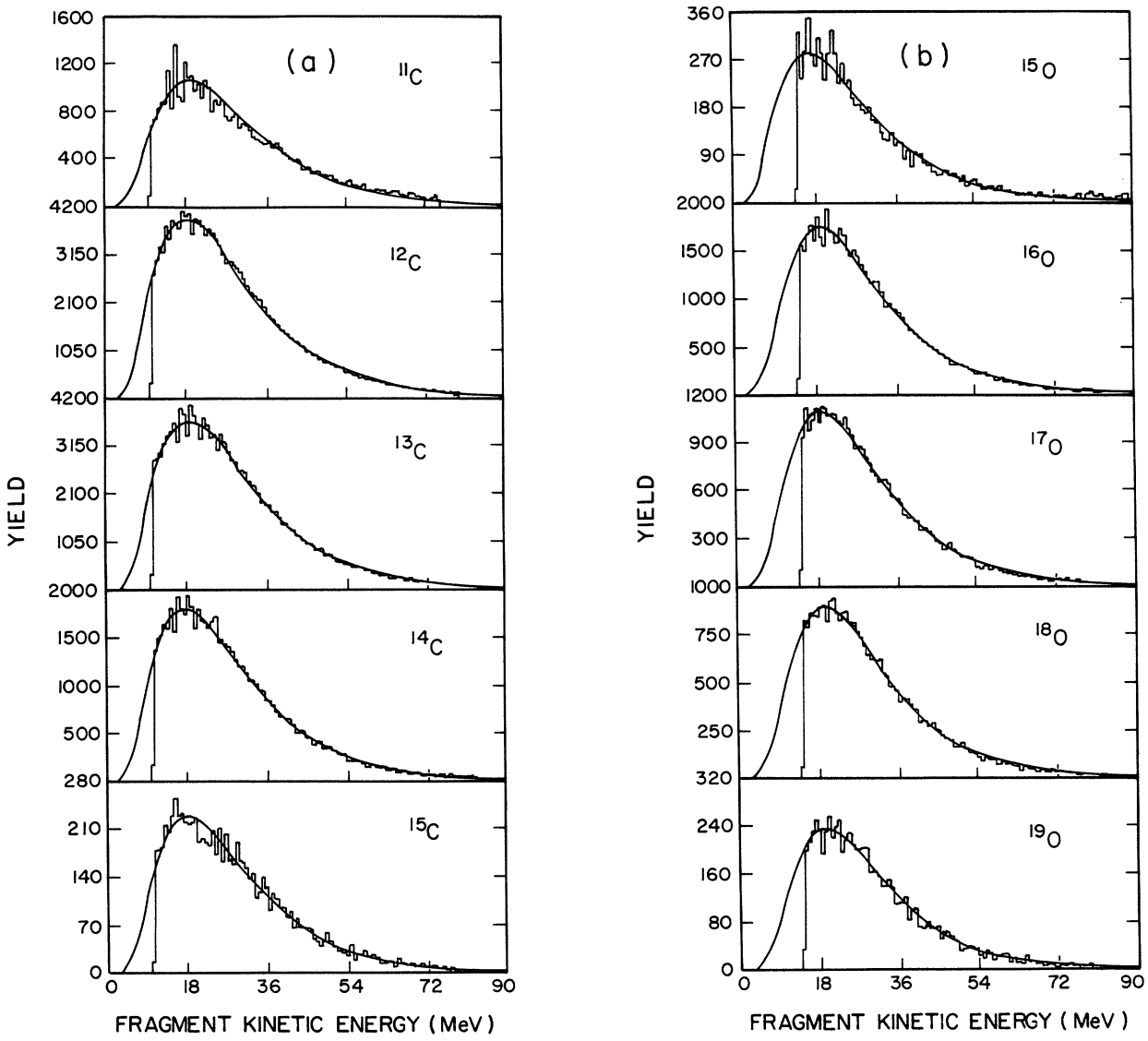

FIG. 7. Kinetic energy spectra of the carbon and oxygen isotopes produced in p-Kr [(a) and (b)] and p-Xe [(c) and (d)] collisions. The solid curves represent the fits as discussed in the text.

same whether these events are observed with a fragment trigger ($A=20$—40) or not. In other words, the trigger requirement of a fragment in the mass range 20—40 does not select a different mechanism for the light fragments, and thus, the inclusive data result from the same reaction mechanism as the coincident data.

The solid line in Fig. 8 represents a power law fit to the data, exclusive of the points at mass 8, 9, 10, and 11. Smooth power behavior obtains when the binding energy per particle is approximately constant. It is clear that even without the mass = 1 point, the data do not favor an exponential. The value of the power law exponent, τ, is about 2.6 ± 0.2 for both target gases.

We have refrained from quoting a chi-square per degree of freedom for the following reason. The statistical errors of the data in Fig. 8 are small ($1/\sqrt{N}$). However, we are fitting a smooth function to data which are manifestly not smooth in order to extract the underlying trend. Thus, performing a weighted fit to these data gives a large chi-square and does not properly measure the uncertainty in the parameter τ. We note, however, that a change of 0.2 in τ produces a change in yield of 1.8 at $A_f=20$, according to Eq. (1).

Although the data in this experiment were obtained at one laboratory angle (34°), an earlier experiment[6] demonstrated that the angular distributions of the fragments $3\leq Z_f\leq 13$ are consistent with isotropy in a system moving along the beam direction with a speed $v/c\sim0.002$ (0.007) for a xenon (krypton) target. Thus, we expect the power law to hold for the fragment's total cross section.

Since our first report,[7] the power law behavior of light fragments $4\leq A_f\leq 24$ has also been observed by Gutbrod *et al.*[22] in reactions between relativistic light projectiles such as Ne and heavy targets, Au and U. These data also

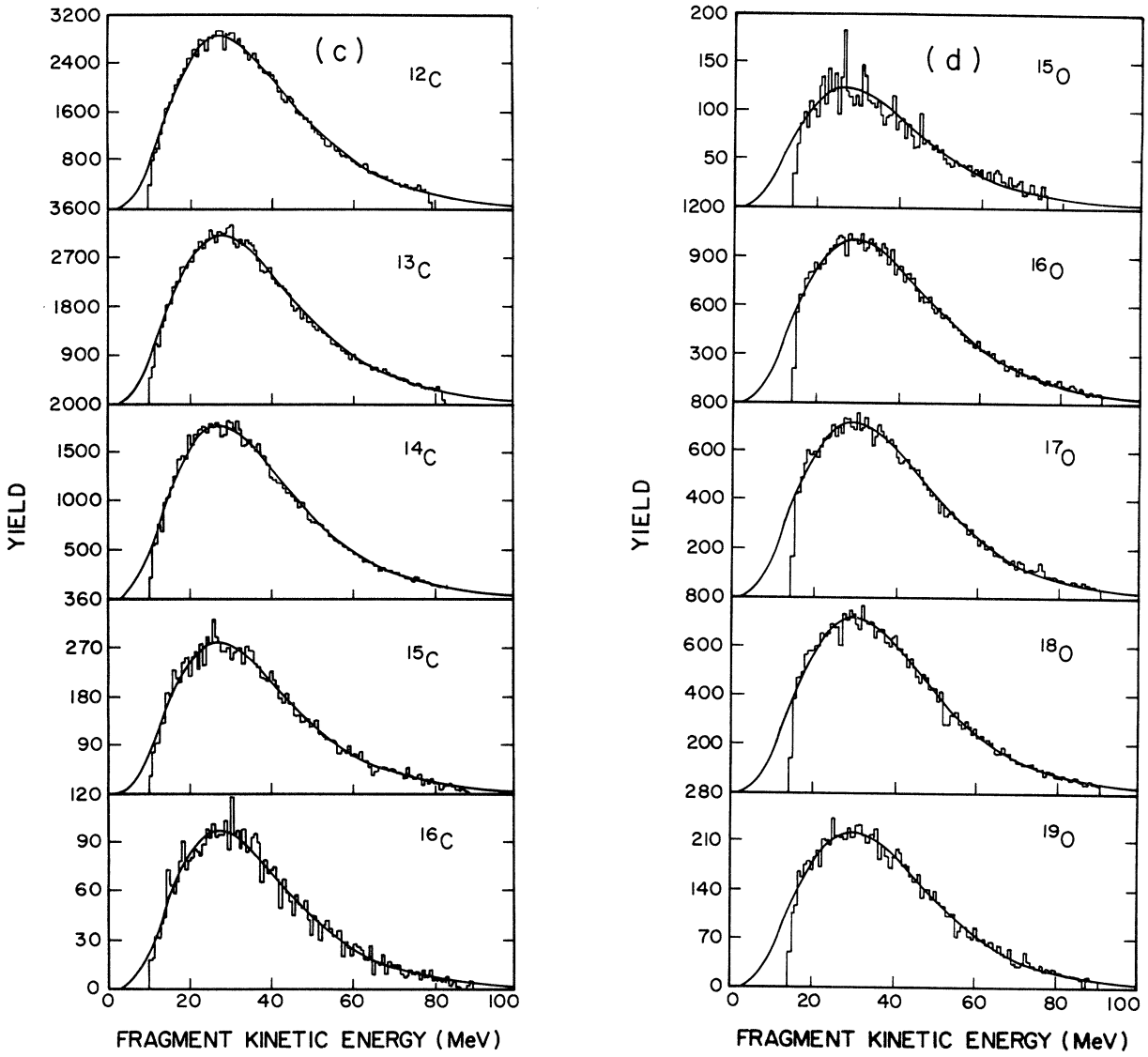

FIG. 7. (*Continued*).

indicate a best fit value for $\tau \sim 2.6$. Thus, it appears that a condensation picture is capable of describing the yield of fragments for both proton-nucleus and nucleus-nucleus collisions. Since the cross section for fragment production is large, on the order of one third of the geometric cross section, the correct parametrization of these data is important for our general understanding of high energy nuclear reactions.

It is well known[9,23,24] that many diverse systems in nature are characterized by power law behavior near their critical point. To be specific, a system undergoing a liquid-gas phase transition at its critical point is expected to form clusters whose frequency of formation, m_l, depends on the number, l of droplets within the cluster as[10]

$$m_l \propto \frac{1}{l^{\tau}} . \tag{3}$$

On very general grounds, the exponent of the power law, τ, is expected to lie within the range of 2–3.[10] The observation that fragments obeyed a power law within an exponent τ of about 2.6 encouraged us to envisage fragmentation as a critical phenomenon. From this viewpoint, fragments are produced in proton-nucleus and nucleus-nucleus collisions when the struck target is brought near its critical point. The critical point is characterized by density fluctuations which are on the order of the size of the system. Furthermore, at the critical point, the contributions to the droplet free energy from surface energy and surface entropy cancel,[10] so the system will disassemble under the influence of the Coulomb repulsion. This model has been discussed in some detail previously, and here we present only a brief summary.[7,8,25]

B. Fragment isotopic yields

In the Fisher droplet model, the relative probability for the occurrence of a cluster containing l constituents depends on the Helmholtz free energy of the cluster. Away

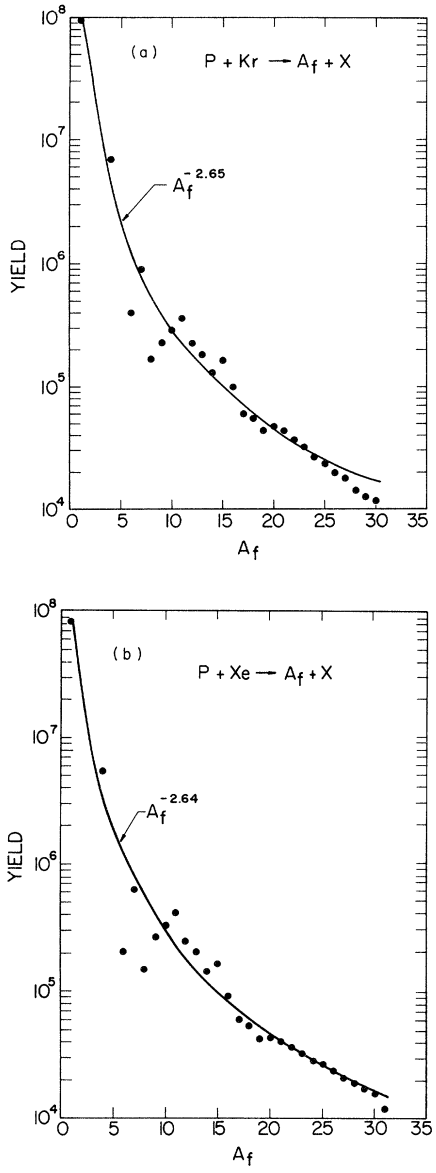

FIG. 8. Fragment mass yield vs A_f for (a) p-Kr and (b) p-Xe collisions. The solid curve is a power law fit to the data.

from the critical point, the droplet formation probability at temperature T will depend on the droplet free energy f_l as

$$m_l \propto l^{-\tau}\exp[-(f_l-\mu l)\beta] , \tag{4}$$

where $\beta=1/T$ and μ is the chemical potential per particle. The preexponential factor has been removed from the free energy, following Fisher. The factor τ is independent of cluster size. The Helmholtz free energy,

$$f_l=U(l)-TS(l) \tag{5}$$

expresses the tradeoff between cluster binding energy $U(l)$ and cluster entropy $S(l)$. Fisher made plausible assumptions about the analytic form of each of these contributions.[10] One expects there to be in each a bulk term, proportional to the number of constituents, and a surface term, proportional to the surface area of the cluster. At the critical point, cancellation occurs between terms in f_l and the chemical potential, leaving only the power law term.[10]

The first step in applying Eq. (4) to nuclei is to generalize a single component model to two components. Thus, we made the replacement in (4)

$$\mu\beta l \rightarrow (\mu_N N_f+\mu_Z Z_f)\beta+\left\{N_f\ln\frac{N_F}{A_f}+Z_f\ln\frac{Z_f}{A_f}\right\} , \tag{6}$$

where μ_N, μ_Z, N_f, Z_f, and A_f denote the neutron and proton chemical potentials, the neutron number, proton number, and nucleon number of the fragment, and the braces contain the entropy of mixing.

To obtain an analytic form for the Helmholtz function, Fisher considered there should be both bulk and surface contributions to f_l, i.e.,

$$f_l=a_v(T)l+a_s(T)l^{2/3} , \tag{7}$$

where a_v and a_s are volume and surface independent constants but are functions of the temperature, T. From the definition of f_l it is obvious that both a_v and a_s contain contributions from the binding energy and entropy of the cluster. We argue that the functional dependence of the entropy of an l nucleon cluster on the variables that describe the system is identical to that of the energy U. Thus, we conjecture that the analytic form of the Helmholtz function is the same as that of the binding energy. The functional form of the binding energy for Z_f protons and A_f nucleons is given by Weizsäcker's semiempirical mass formula

$$f(Z_f,A_f)=a_vA_f-a_sA_f^{2/3}-a_CZ_f^2/A_f^{1/3} -a_a(A_f-2Z_f)^2/A_f-\delta , \tag{8}$$

where $\delta=a_p/A_f^{0.75}$ for odd-odd nuclei, zero for odd-even nuclei, and $-a_p/A_f^{0.75}$ for even-even nuclei. The coefficients in (8) represent the volume, surface, Coulomb, symmetry, and pairing contributions to the free energy. At $T=0$, these coefficients assume their nominal values. Substituting (6) and (8) into (4) we obtain the TLDM expression for the isotopic yield

$$Y(Z_f,A_f)=\frac{C}{A_f^{\tau}}\exp\left\{[f(Z_f,A_f)+\mu_N N_f+\mu_Z Z_f]\beta + N_f\ln\frac{N_f}{A_f}+Z_f\ln\frac{Z_f}{A_f}\right\} . \tag{9}$$

It must be emphasized that while the parametrization of f is the same as that of the empirical mass formula, the coefficients contain contributions from both the binding energy and the entropy of the cluster of Z_f protons and N_f neutrons.

The fragment data from each target were fit with this expression (Fig. 9). In all, the yields of about 60 isotopes from each target were fit with one set of parameters. The values of the fitted parameters are listed in Table V. We know that the mass fomula is not capable of reproducing

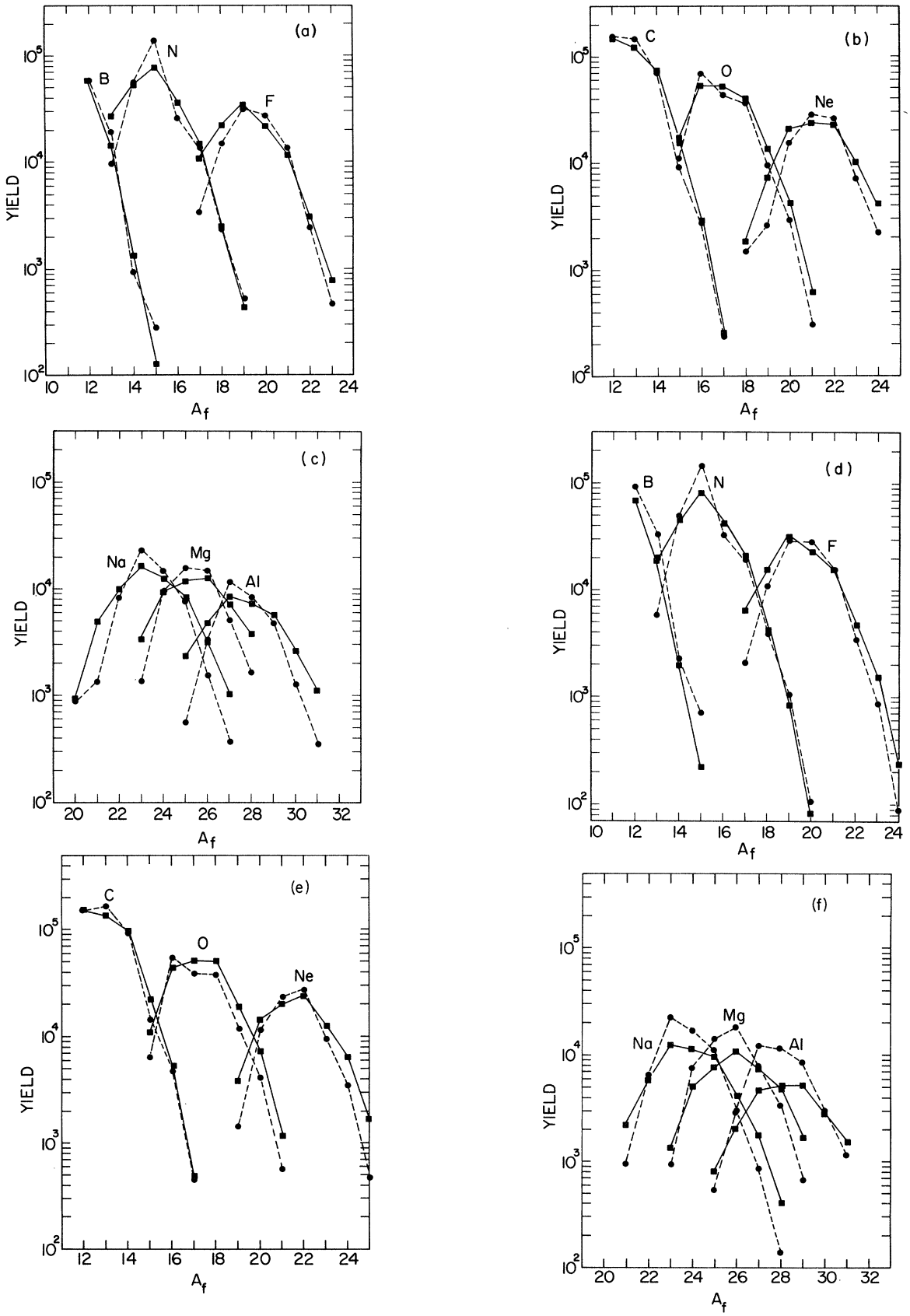

FIG. 9. Isotopic fragment yields produced in (a)—(c) p-Kr and (d)—(f) p-Xe collisions. Circles represent the data, while squares are the fit according to Eq. (9). The dashed and solid lines are drawn to guide the eye.

TABLE V. Values for the parameters in the fits to the isotopic yields.[a]

Parameter	Xe	Kr	Nominal value
Volume a_v (MeV)	14.1	14.1	14.1
Surface a_s (MeV)	5.35	6.61	13.0
Coulomb a_C (MeV)	0.489	0.400	0.595
Symmetry a_a (MeV)	22.66	23.30	19.0
Pairing a_p (MeV)	5.92	5.28	33.5
Proton chemical potential μ_p (MeV)	−11.32	−11.01	
Neutron chemical potential μ_n (MeV)	−7.59	−7.62	
Temperature $1/\beta$ (MeV)	3.28	3.24	
Power law exponent τ	2.64	2.65	

[a]The values above have been calculated by setting the volume free energy equal to 14.1 MeV. Assuming a volume heat contribution of 8 MeV to the volume free energy, we find $1/\beta \sim 5$ MeV and the parameters a_s, a_C, a_p, μ_p, and μ_n, given in the table, should be scaled up accordingly.

the exact variations in binding energy for nuclei between hydrogen and carbon, and therefore do not expect perfect fits. While the Weizsäcker parametrization represents the average behavior, the data, of course, contain fluctuations about the theoretical curve.

If the result of the proton-nucleus collision is a system which is near its critical point, we would expect that the function $f(Z_f,A_f)$ would just balance the chemical potential terms in (9). Using the values for xenon listed in Table V and calculating each of the above quantities for ^{4}He and ^{20}Ne, we find nearly exact cancellation. We expect, based on this model, that above and below the critical temperature the isotopic yield, $Y(Z_f,A_f)$, would be exponentially damped relative to the yield observed at T_c.

If we compute the argument of the exponential in (9) for a nucleus such as ^{18}N, we find that the power law term is reduced by a factor of $\sim\frac{1}{100}$. This behavior is quite evident in Fig. 9, where we see a dramatic falloff in yield away from the most abundantly produced isotope of a given species. The symmetry energy term, i.e., the $(A_f-2Z_f)^2/A_f$ term in (8), dominates the expression which chooses the most abundant isobar for a given A_f.

Since the data determine only the products $f\beta$ and $\mu\beta$, we cannot uniquely set the temperature scale without additional information. If we ignore the heat contribution, TS, to the bulk free energy and require a_v to be equal to its value in normal nuclear matter, we obtain a critical temperature for finite nuclei of about 3 MeV for both the xenon and krypton targets. Alternatively, we may estimate that at most we could have added an amount of heat equal to the average nucleon removal energy, about 8 MeV, to the bulk binding energy; with this provision, T_c increases to about 5 MeV. However, one must recognize that these estimates ignore the density and temperature dependence of both the binding energy and entropy per nucleon.

We note that in the one-component Fisher model the surface contribution to the free energy is supposed to go to zero at the critical point. This comes about because of cancellation between the surface energy and surface entropy. Although our surface coefficient, a_s, is small and reduced from its value (see Table V) pertaining to ground state nuclei at $T=0$, it is not zero. On the other hand, Fisher's model did not account for the Coulomb force. In fact, he considered only short range attractive forces. The surface tension must balance the repulsive Coulomb force in the remnant system, and therefore the system will disassemble before there is exact cancellation between the surface energy and surface entropy terms.

Both Xe and Kr show a large value for the symmetry energy term in Eq. (8). The symmetry energy contribution to $f(Z_f,A_f)$ is opposite in sign to the bulk binding energy term a_v, and therefore this increase favors $N=Z$ fragments in the remnant system. The coefficient of the pairing term is greatly reduced over its nominal value. This is to be expected in a system near its critical point when $1/\beta \gg \delta$, the pairing energy. The value of the neutron chemical potential is close to the value expected for normal nuclei, $\mu_N(T=0)\sim -8$ MeV. The proton chemical potential is about 3 MeV lower than this, owing to a contribution from the mean Coulomb field in which the protons move. Estimates using a uniform charge distribution within the remnant system indicate that the observed 3 MeV effect is reasonable.

C. Fragment kinetic energy spectra

Individual kinetic energy spectra were fit using a functional form significantly different from those used in previous experiments. Data from earlier experiments[4–6] emphasized those fragments whose energies were greater than or approximately equal to the most probable energy observed. Data below this peak energy, which occurs at about 1–2 MeV/nucleon, are difficult to observe because of experimental cutoffs. Our detector system, which has a cutoff of about $0.5A$ MeV, was designed specifically to observe fragments below the most probable kinetic energy. Thus, the functional form which worked well in the absence of low energy data was found to be inadequate. Previous data have been fit to a distribution given by[5]

$$\frac{d^2\sigma}{dE\,d\Omega}=N(E/E^*)^{1/2}(E^*-B)^{1/2}e^{-(E^*-B)/T'}, \quad (10)$$

where

$$E^*=E+\tfrac{1}{2}M_f\beta^2-2\sqrt{E}\sqrt{(1/2)M_f\beta^2}\cos\theta,$$

$\beta=v/c$, and E is the laboratory kinetic energy. The fragments are viewed as having been emitted from a remnant system of the proton-nucleus collision containing A_R nucleons recoiling along the beam direction with speed v. The fragment is observed at laboratory angle θ and kinetic energy E. The parameter E^* represents the fragment energy in the rest frame of A_R. The distribution (10) follows from the transformation along the beam direction of a Maxwell-Boltzmann distribution in the rest frame of the excited remnant. The parameter T', therefore, is related

to the mean square momentum of fragment A_f in this frame.

The Coulomb repulsion energy between Z_f and the remaining $Z_R - Z_f$ nucleons is usually expressed in terms of a fraction of the tangent sphere value, $B = KB_{TS}$, $K < 1$, and

$$B_{TS} = \frac{e^2 Z_f (Z_R - Z_f)}{r_0 [A_f^{1/3} + (A_R - A_f)^{1/3}]} . \tag{11}$$

For convenience, r_0 is usually taken equal to 1.44 fm, thus cancelling the factor of e^2. The data consistently show that the Coulomb energy is a fraction of that expected for tangent spheres.[4-6]

An earlier experiment by the Purdue group, utilizing telescopes comprised of silicon surface barrier detectors, provided evidence that fragments of carbon and those heavier had been emitted from a common system which was a remnant of the initial proton-target collision.[6] The target nuclei studied in that experiment were the same as those studied in the present paper, as was the incident energy range. Data were taken at laboratory scattering angles between 34 and 76 deg. The nature of that detector system did not permit isotopic separation except for the lightest fragments, nor did it allow the detection of fragments with kinetic energies substantially below the peak in the distribution. However, by fitting the spectra of all the fragments from a given target with Eq. (10), we were able to draw several conclusions concerning the nature of the remnant system which emitted the fragments. The Doppler shift of the energy spectra as a function of laboratory angle indicated that the fragments had been emitted isotropically in the rest frame of the remnant, which was recoiling with a small velocity along the incident proton direction. It was found that $v(\mathrm{Kr}) = (0.007 \pm 0.001)\, c$ and $v(\mathrm{Xe}) = (0.002 \pm 0.001)\, c$.[6] This component of remnant velocity contributes very little to the kinetic energy of the fragment in the laboratory.

The high energy tails of the Maxwell-Boltzmann-type kinetic energy spectra are characterized by the slope parameter T'. When T' is plotted (Fig. 10) versus fragment mass number, A_f, a linear relationship between T' and A_f for fragments heavier than boron becomes apparent. If a fragment of mass A_f is emitted from a system of mass A_R which is at rest, the conservation of momentum between the observed fragment and the rest of the system $(A_R - A_f)$ is given by the factor $\nu = (1 - A_f/A_F)^{-1}$. The linear relation between T' and A_f indicates that *all of the fragments originate from a common remnant reduced in nucleon number from the target* and that this remnant is characterized by a quantity T defined by

$$T' = \frac{T}{\nu} = T\left[\frac{A_R - A_f}{A_R}\right] . \tag{12}$$

Figure 10 shows that the value for krypton is about 14.2 MeV, in good agreement with the value obtained in an earlier experiment (see Table VI).[6]

We expect that T is related to the mean square nucleon momentum within the remnant system. Fragments emerge from the remnant system as an agglomeration of A_f nucleons. Within the remnant, the average nucleon momentum $\langle \vec{p} \rangle = 0$, while the mean square nucleon momentum has some nonzero value, $\langle \vec{p}^{\,2} \rangle = \sigma \neq 0$. It follows from the mean value theorem that the quantity $\langle \vec{p}^{\,2} \rangle$ is related to T,

$$T = \frac{2}{3} \frac{\langle \vec{p}^{\,2} \rangle}{2M_N} . \tag{13}$$

Goldhaber[26] has pointed out that the fragment momentum distribution is not sensitive to the manner of fragmentation of the rest of the nucleus, and one obtains the result (13), whether the process is fast and does not involve thermal equilibrium, or slow, occurring after a rough equilibrium has been established.

Using an ideal Fermi gas model, we can relate $\langle \vec{p}^{\,2} \rangle$ to the Fermi momentum, p_F, by

$$p_F^2 = \tfrac{3}{5} \langle \vec{p}^{\,2} \rangle . \tag{14}$$

Thus,

$$T = \frac{1}{5} \frac{p_F^2}{M_N} . \tag{15}$$

We note that the values found for T for the xenon and

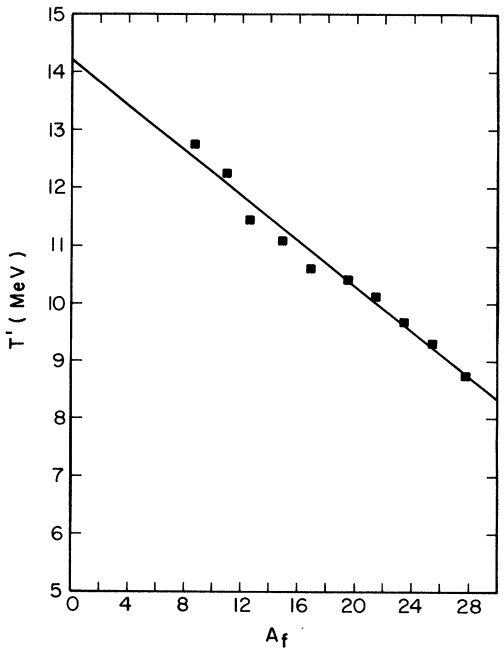

FIG. 10. Inverse logarithmic slope parameter T' vs A_f for fragments produced in p-Kr collisions.

TABLE VI. Parameters fixed in the fits to the isotopic kinetic energy spectra.

Parameter	Xe	Kr
Slope T (MeV)	15.0	14.0
Remnant mass A_R	110	75
Velocity β (in beam direction)	0.002	0.007
Temperature T_c (MeV)	3.28	3.24
Remnant charge Z_R	47	32

krypton targets are in good agreement with the values we calculate using Eq. (15) and p_F obtained from electron scattering experiments.[27]

In summary, the implication of the linear relation between T' and A_f is *that fragments heavier than boron are emitted from a common remnant characterized by the parameter T.* One possible interpretation of T is that it reflects the nucleon mean square momentum in the remnant system. Since the value of T for both targets is approximately that expected for ground state nuclei, and it greatly exceeds the value of T_c determined by the isotopic data, *we conclude that the high energy tails of the kinetic energy distributions are dominated by this nonthermal contribution.*

The kinetic energy spectra obtained in the present experiment differ significantly from those in the previous experiment. The use of the gas ionization detector and the time-of-flight system enabled the isotopic separation of fragments down to a kinetic energy of about 5 MeV. On the other hand, a substantial fraction of the energy spectrum of fragments lighter than boron produced from the xenon target are too energetic to be stopped in the gas detector, prohibiting a study of their high energy tails.

In those cases where data near and below the peak have been observed, it has been customary to introduce a smearing of the Coulomb tangent sphere fraction in order to broaden the function to fit the data. This smearing has often been attributed to possible distortion in the nuclear shape at the time of fragment emission. However, a consistent description of the fragment kinetic energy spectrum is achieved if we envisage that rather than being surface dominated, fragmentation is a volume dominated effect. Thus, a heavy fragment is more likely to be formed near the center of the nucleus where the density is higher, rather than in the diffuse surface. The reduction in the Coulomb energy arises then from two possible effects: expansion of the condensing system at the time of fragment formation, and the position dependence of the Coulomb energy within the remnant volume. The fragment kinetic energy spectra must contain information regarding these Coulomb effects, as well as information on Fermi momentum, the temperature at which the condensation occurs, and momentum conservation.

The kinetic energy spectra were fit by convoluting the distribution (10), where $T'=T/\nu$ with T fixed at the Fermi momentum equivalent temperature (15), with a Maxwell-Boltzmann distribution in which the temperature T_c was fixed at the value determined from the fit to the isotopic data (see Table VI). The laboratory distribution was given by[14]

$$\frac{d^2\sigma}{dE_f d\Omega}(Z_f,A_f,E_f,B)=N\left[\frac{E_f}{E^*}\right]^{1/2}\int_0^{E^*-B}\epsilon^{1/2}(E^*-B-\epsilon)^{1/2}\exp[-(\epsilon/T-(E^*-B-\epsilon)/T_c)\nu]d\epsilon\ . \tag{16}$$

The Coulomb repulsion energy B was described by a probability distribution, $P(B)$, characterized by two parameters, B_0 and σ. The data demanded that $P(B)=0$ at $B=0$. This can be justified if we assume that the distribution for B is related to the position within the remnant at which the fragment is born. Phase space considerations then require the above condition at $r=0$. Thus,

$$P(B)dB=\sqrt{B}\exp\left[-\frac{(B-B_0)^2}{2\sigma^2}\right]dB\ . \tag{17}$$

Finally, then, the function (16) weighted by the distribution (17) was integrated over B from zero to the smaller of E^* or B_{TS}. This function produced the fits shown in Fig. 7. Note that only three parameters for each spectrum are fit, while all other parameters are held fixed at the values determined previously. The average χ^2 per degree of freedom was 1.5. Only statistical errors were used in these fits.

A systematic trend in the fitted Coulomb parameters becomes evident when these are studied as a function of the fragment's charge. Rather than B_0 we have used the more physical most probable value of the Coulomb energy, B_{MP},

$$B_{MP}=\tfrac{1}{2}[B_0+(B_0^2+2\sigma^2)^{1/2}]\ . \tag{18}$$

In Fig. 11 we have plotted $B_{MP}(Z_f)$ for the xenon and krypton targets. The data have been systematized by fitting each parameter, $B_{MP}(Z_f)$ and $\sigma(Z_f)$ to a cubic function of Z_f. The parameters of this fit are given in Table VII. We note that for both the xenon and krypton targets the values of $B_{MP}(Z_f)$ are about one tenth of the tangent sphere values, and thus the fragments from these targets have very little Coulomb energy. About 80% of the observed fragments from xenon have Coulomb energies less than half of the value of tangent spheres.

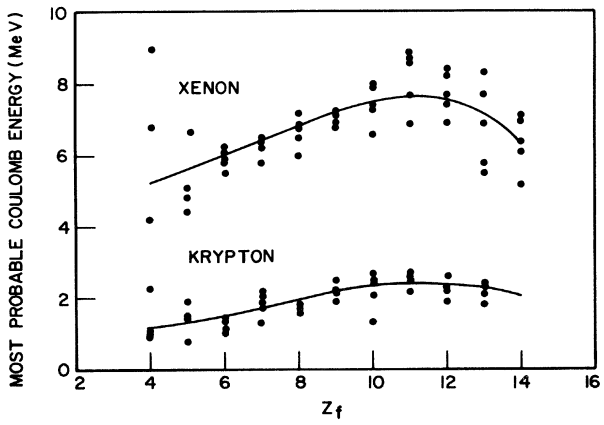

FIG. 11. Most probable Coulomb energy versus fragment charge, Z_f, for p-Kr and p-Xe collisions. The solid curves are fits to the data according to the equation in Table VII.

TABLE VII. Coefficients for Coulomb energy probability function.

Peak energy (MeV)$=A_1+A_2Z_f+A_3Z_f^2+A_4Z_f^3$
Width energy (MeV)$=B_1+B_2Z_f+B_3Z_f^2+B_4Z_f^3$

Parameter	Xe	Kr
A_1	6.37	1.11
A_2	−0.915	−0.178
A_3	0.197	0.0587
A_4	−0.00941	−0.00293
B_1	10.5	2.39
B_2	−0.609	−0.342
B_3	0.409	0.164
B_4	−0.0232	−0.00844

We can formulate a very simple model for relating the Coulomb energy to a position inside the remnant of the proton-nucleus collision at which the fragment is formed. The fragment is assumed to be formed at some location R inside of a uniform spherical charge distribution at normal nuclear density. The charge outside of the sphere of radius R is assumed to expand uniformly during fragment emission so that it has no influence on the Coulomb repulsion energy of the fragment (Fig. 12). The fragment's kinetic energy in the center of mass system owing to Coulomb repulsion is given by

$$E_K(R)=\frac{Z_fZ_Re^2}{R_R^3}(R^2+3RR_f)(1-A_f/A_R)^2 . \quad (19)$$

We can solve this expression for the fragment formation position R from the remnant center as a function of the measured Coulomb energy:

$$R(E_K)=\tfrac{1}{2}(9R_f^2+4C)^{1/2}-\tfrac{3}{2}R_f , \quad (20)$$

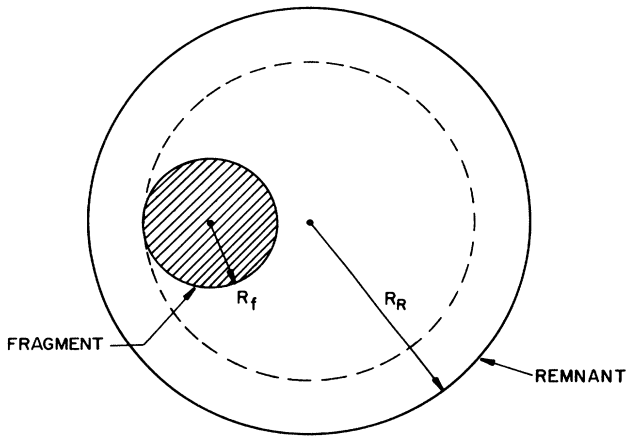

FIG. 12. Geometric model relating Coulomb energy to location within remnant volume at which the fragment is formed.

where

$$C=\frac{R_R^3}{Z_fZ_Re^2(1-A_f/A_R)^2}E_K . \quad (21)$$

The values of R corresponding to the peak of the

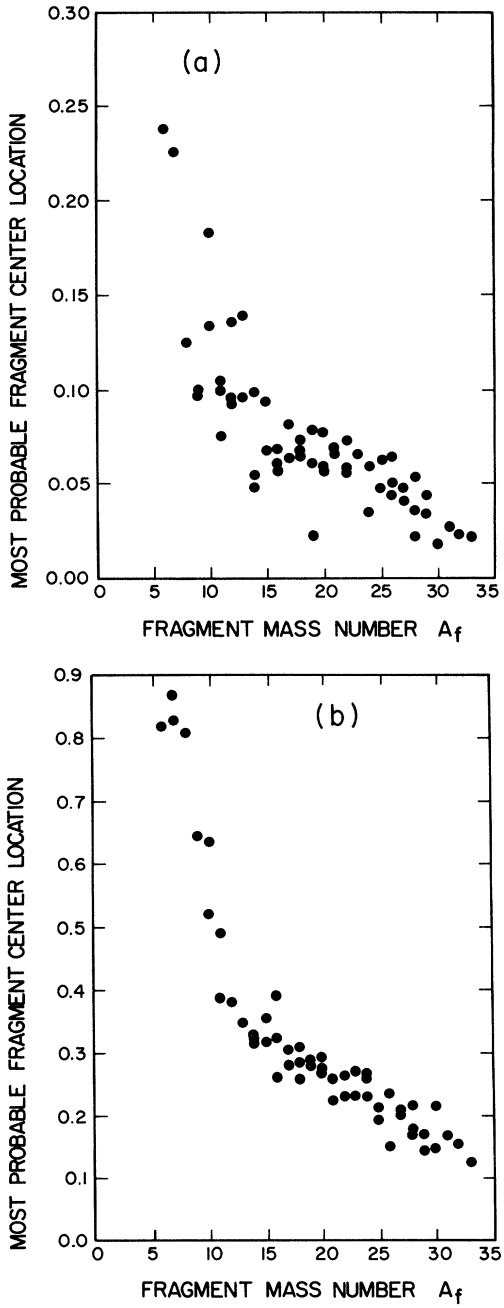

FIG. 13. The location within the remnant at which the fragment of mass A_f is formed based on the most probable Coulomb energy and the simple model, as discussed in the text. The vertical scale should not be taken literally, but does suggest a correlation between fragment mass number or size and the location where the fragment is most likely to be formed within the remnant. (a) p-Kr fragments; (b) p-Xe fragments.

Coulomb energy distribution are plotted in Fig. 13. The pattern observed in these plots indicates that the larger fragments are formed closer to the center of the remnant as the fragment mass number A_f increases. This behavior is expected in the TLDM model. Droplets, or nuclei, are formed as a result of density fluctuations. Therefore, the center of the remnant system is favored over the diffuse edge for forming large droplets. Furthermore, a fragment such as oxygen requires about 50% of the available linear dimension when formed in a remnant of mass 100, assuming normal nuclear density. Thus, the larger the fragment, the more likely it is to be formed close to the center of the remnant for this geometrical reason.

If the power law is to be obeyed, the remaining light nuclei must necessarily be formed in the remnant's surface. If, as is likely, the remnant system undergoes some expansion prior to its breakup,[28] the reduction in density again favors the formation of the heavy fragments in the center of the system. Unfortunately, our data do not permit us to determine unambiguously what part of the fragment's Coulomb energy is owing to location within the remnant and what part is owing to expansion of the remnant system. Only a study of the whole event can, in principle, determine the size of the remnant system.

The power law (1) gives the relative probability for the occurrence of a droplet containing m_l constituents. We can use the information contained in the power law fit to our data to calculate the mean multiplicity expected in the breakup of a remnant of A_R nucleons. For example, if the remnant contains 84 nucleons and $\tau=2.65$, the average event multiplicity is about 55, with the average fragment size $84/55\sim1.5$. The mass = 1 multiplicity is about 40, approximately half of which are expected to be neutrons. In relating the excitation energy of the remnant to the observed temperature, T_c, we must take into account the reduction by 1.5 of the number of degrees of freedom. The power law also contains information regarding the width of the multiplicity distribution.

IV. DISCUSSION

We have interpreted the observation that the fragment mass yield obeys the power law of Eq. (1), with τ about 2.6 for a wide range of both target and projectile mass and incident energy, as an indication that fragments are formed in an excited nucleus near its critical point. Our quantitative description of fragment production is based upon the analogy between a highly excited nucleus and a hot van der Waals gas. The classical theory as developed by Fisher, describing the liquid-gas phase transition in a single component substance, has been modified in order to treat nuclei. The main ingredients in Fisher's theory are the following: (1) an attractive short range force and a hard core repulsion; (2) a Helmholtz free energy for droplet formation which could be decomposed into two contributions, one pertaining to the bulk of the liquid and the other to its surface; and (3) a parameter τ which provides the power law behavior at the critical point. Although the existence of τ was asserted rather than proven by Fisher, it is now well established that real gases do indeed display the predicted power law behavior with τ within the range 2–3 expected on theoretical grounds.[9]

Pursuing the above analogy, it is natural to use the liquid drop model to describe the nucleus. At temperature $T=0$ the free energy of a nucleus is identical to the Wiezsäcker semiempirical mass formula. At temperatures above zero, we have also employed the Weizsäcker formulation but with two important distinctions. First, the expression now represents the Helmholtz free energy of the nucleus at temperature T, and therefore contains contributions from both the volume and surface entropy. We have assumed that the former contribution depends on the number of nucleons in the fragment, A_f, and that the latter depends on $A_f^{2/3}$. Second, the coefficients in the free energy parametrization are *temperature* and *density* dependent.

In addition, we have had to account for the presence of two nucleon species, whereas Fisher's model considered only a single homogeneous substance. Thus, we have introduced both a neutron and a proton chemical potential and the additional contribution to the entropy of the fluid owing to mixing.

Fitting the isotopic yield data using this description permits the determination of the ratio of the abovementioned parameters to the temperature of the system. It is interesting to note that one cannot determine the temperature at the critical point in a single component system by simply measuring the cluster yield. In this case, the isotopic yield is the same as the mass yield. Thus, the isotopic "thermometer" is lost. It is the isotopic yield which reflects the temperature of the system from this point of view.

In the thermal liquid drop model of fragment production, several factors contribute to a fragment's kinetic energy spectrum. Because of relatively low temperatures, $T_c\sim5$ MeV, it seems natural to attribute the 14 MeV exponential tails of the kinetic energy spectra to the mean square momentum of a nucleon in the cold target (fermions in a box). This equivalent temperature for a heavy nucleus is on the order of 14 MeV and is much larger than the thermal contribution of about 5 MeV as determined from the isotopic yields. Our description of fragmentation is in marked contrast to earlier models in which the phenomenon was treated as a surface evaporation. The droplet picture requires that the entire volume of the excited remnant participate in the formation of fragments. As fragments are formed, with a probability which on the average obeys the power law, the system disassembles under the influence of the Coulomb repulsion. It is expected then that Coulomb energies will be substantially less than expected on the basis of tangent sphere estimates. The data are consistent with this picture, and one may also conclude from the simple model presented in Sec. III C that a heavy fragment is more likely to be formed in the center of the remnant system.

Our modified version of Fisher's model (TLDM) is surprisingly successful in describing the data. This success may be more attributable to the general features of a

system near its critical point than to the particular description we have chosen. For example, comparing the values of τ obtained from percolation calculations[24] to those inferred from measurements using real gases,[9] we may conclude that the detailed nature of the interactions involved alter τ only slightly. Thus, it may be that the essential quantities necessary to describe a liquid-gas system near its critical point, namely τ and the cluster free energy, have been correctly identified by Fisher. Fisher's formulation ruled out long range forces and neglected the interaction between clusters. Hence, it might appear that the presence of the Coulomb force would necessitate substantial modification of the model. However, since the total Coulomb energy in these fragments ($A \leq 35$) is much less than the total binding energy, it may not significantly alter the basic description. As it affects the interactions between fragments, the Coulomb force promotes the disassembly of the excited remnant before a full cancellation between surface energy and surface entropy occurs. The stability of a nucleus in the liquid drop model results from competition between surface tension and Coulomb repulsion. Thus, disassembly can occur at a temperature somewhat below T_c, before the surface thermodynamic potential is identically zero. An estimate using the parametrization of the surface thermodynamic potential given by Ravenhall *et al.*[29] and a $T_c = 5$ MeV shows that instability occurs when the temperature is above 4 MeV.

The basic result of Fisher's model is that, at the critical point, the fluid can be described as if comprised of an ideal gas of noninteracting clusters, where the partial pressure owing to the clusters of a given size is given by its concentration, i.e., the power law (1). It is consistent with the description of fragmentation as a critical phenomenon that we use this classical model for the following reason. The power law distribution describing the fragment yield implies that clustering has occurred. Since clustering requires collisions, there must be substantially less Pauli blocking in the excited nuclear remnant than in ground state nuclei. In this case, a classical description of the remnant may be more appropriate than that of a degenerate Fermi gas at a temperature that is small compared to E_f.

A parameter which is relevant to the fragmentation process is the freezeout density, ρ_f, the density at which collisions between fragments cease. It has been pointed out by Curtin *et al.*[30] that the relation of the freezeout density to the critical density, ρ_c, is important in correctly determining T_c. If freezeout occurs at densities less than the critical density, then one tends to underestimate T_c. For freezeout densities greater than the critical density, T_c is correctly determined. The degree of error in the former case depends on ρ_c and ρ_f and on the shape of the coexistence curve. There seems to be a general consensus, however, that both densities are in the neighborhood of $0.5\ \rho_0 \rightarrow 0.3\ \rho_0$, where ρ_0 is normal nuclear density. One could argue that freezeout must occur at densities less than ρ_c for the following reason. Near the critical temperature and density, the correlation length is on the order of the size of the system, that is, density fluctuations are not localized, but occur throughout the entire volume. The formation of clusters according to the power law (1) indicates that the system has passed near the critical point before it disassembles owing to Coulomb repulsion. As it expands, the freezeout density is reached and the fragment distributions are frozen at that time.

Several authors have recently taken different approaches in calculating the thermodynamic properties of hot nuclear matter. Ravenhall, Pethick, and Lattimer have used a microscopic Hamiltonian based on the Skyrme force to calculate both the bulk and surface properties of a nucleus at temperature T.[29] An important feature of their model considers a hot nucleus in equilibrium with its vapor of nucleons. They find that the critical temperature is between 15 and 20 MeV. A calculation by Jaqaman, Mekjian, and Zamick also employs the Skyrme interaction and finite temperature Hartree-Fock theory.[31] They estimate that the critical temperature is in the neighborhood of 20 MeV for infinite nuclear matter, but drops to about 8 MeV in finite nuclei. It is clear that there is currently no consensus on how one is to construct an equation of state for finite nuclei. As Sauer *et al.* point out, the Skyrme force may be unreliable at temperatures exceeding 6 MeV.[32] A difficulty with the above calculations is that the effect of clustering is not accounted for. All of the above models consider nucleons either in a gas or liquid phase. Friedman and Pandharipande point out, however, that at low densities, $\rho_0/5$, deuteron and alpha clusters make a significant contribution to the free energy, particularly at temperatures less than 5 MeV.[33] It would seem that a complete treatment of the nuclear equation of state would have to allow for such clusters. Since the interaction between a nucleon and a cluster may be considerably different than between nucleons, the equation of state could be affected.[34] A simple argument based on de Boer's law of corresponding states indicates that a gas of alpha clusters may have a critical temperature as low as 3 MeV.[35]

V. SUMMARY AND CONCLUSIONS

We have presented the results of an experiment in which high energy protons (80–350 GeV) bombarded heavy nuclear targets (krypton, xenon). A time-of-flight energy loss spectrometer was used to identify nuclear fragments from helium to aluminum. Fragment cross sections and kinetic energy spectra have been presented as a function of charge and mass. When the fragment yields are summed over charge for a fixed fragment mass, the data obey a power law (1) with an exponent suggestive of a phase transition near the critical temperature and density. Thus, we have been encouraged to treat fragmentation as a condensation or clustering phenomenon, emphasizing the analogy between hot nuclear matter and a van der Waals gas. As in the case of a van der Waals gas, nuclear matter consists of particles (nucleons) interacting with repulsive cores and short-range attractive forces.

We have taken the classical model describing condensation in a single component fluid by Fisher and adapted it to describe nuclei. This model was then used to fit our isotopic data. The basic quantities in this model are the free energy for fragment formation, the neutron and proton chemical potentials, and the temperature of the system

at the time of fragment formation. The data do not uniquely determine the energy scale, since only the ratios of free energy/temperature and chemical potential/temperature are fixed by the data. If we assume that we have added 8 MeV per nucleon to the nucleus, we find that the critical temperature is near 5 MeV.

The fragment kinetic energy spectra provide important evidence that most of the fragments heavier than boron are formed simultaneously in a system significantly reduced in nucleon number from the initial target. We have interpreted the high energy tails of the spectra as reflecting the zero-point motion of a nucleon in this system. This momentum is considerably greater than the contribution owing to thermal motion. Furthermore, the spectra indicate that Coulomb repulsion energies are much smaller than the values expected on the basis of two tangent spheres. This is consistent with our picture of fragmentation occurring within the volume of the excited nuclear remnant.

Although the fragments represent the asymptotic final state of the interaction between a high energy proton and a heavy nucleus, we may speculate on the evolution of the process. Results of a recent experiment by Nakai *et al.*[36] indicate that a 4 GeV hadron will lose a significant fraction of its energy about 30% of the time in a collision with a heavy nucleus. This is in close agreement with the total cross section for fragment production as mentioned in our Introduction. The initial stage of such collisions can be described as producing a forward moving fireball of approximately 20 nucleons which undergoes a rapid decay into nucleons; the remaining nucleus cools while expanding. As the neighborhood of the critical temperature and density is approached, the system, which we have termed the remnant, becomes unstable and decays into the multibody fragment final state. Agreement between the number of nucleons in the fireball determined by Nakai and the mass loss between the initial target and the remnant as inferred by us from the kinetic energy spectra is excellent. This evolutionary sequence is shown schematically in Fig. 14. In a system of finite particle number the critical point may well be more of a neighborhood than a single point. We have indicated by the dashed lines a band in the temperature-density plane that the system may take in its path towards criticality.

We should expect from the TLDM that the critical point can be reached in collisions between heavy ions. Indeed, the same power law behavior as in Eq. (1) has been observed.[22] In addition, we do not expect every hadron or heavy ion interaction with a large nucleus to result in fragments according to (1). Peripheral collisions which leave a small amount of energy in the system will give rise to evaporation of nucleons and light composites. In this case, the mass yield should fall exponentially with increasing product mass number. On the other hand, if sufficient energy is deposited in the nucleus, the yield of fragments should again decrease as it becomes more likely that total vaporization of the nucleus occurs. Events of this type have been observed for both incident protons[37] and heavy ions.[22] Within the description presented here, the production of heavy nuclear fragments according to Eq. (1) is the signature that the critical temperature and density have been approached by the remnant system. Figure 15 indicates schematically the behavior expected in a hadron or heavy-ion—nucleus collision.

In summary, fragmentation is viewed as the multibody breakup of an excited nucleus resulting from the interaction of a relativistic proton and a heavy nuclear target. The disassembly of the remnant of this collision occurs near the critical point of the system, as evidenced by the power law distribution of the fragment mass yield (1). If this description of fragmentation is correct, it should be possible, using the theory of critical exponents,[10,23] to explore the nuclear equation of state near the critical point.

ACKNOWLEDGMENTS

We would like to thank J. Moore and C. Schanke of Purdue University for their help in the telescope construction. We would also like to thank the members of the Ac-

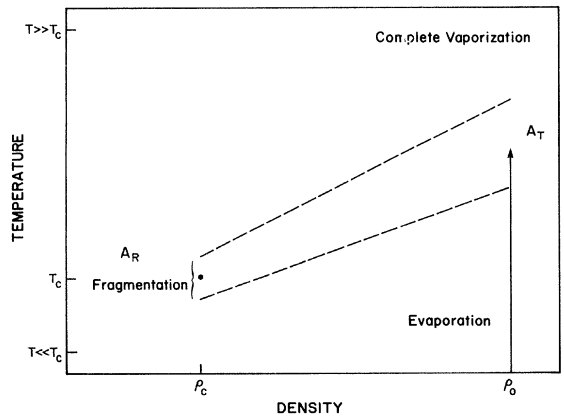

FIG. 14. Qualitative behavior of a high energy hadron/heavy ion-nucleus collision. Three phenomena are represented: evaporation, fragmentation, and vaporization. Fragmentation occurs when the remnant A_R ($<A_{\text{target}}$) is in the neighborhood of the critical temperature T_c and density ρ_c.

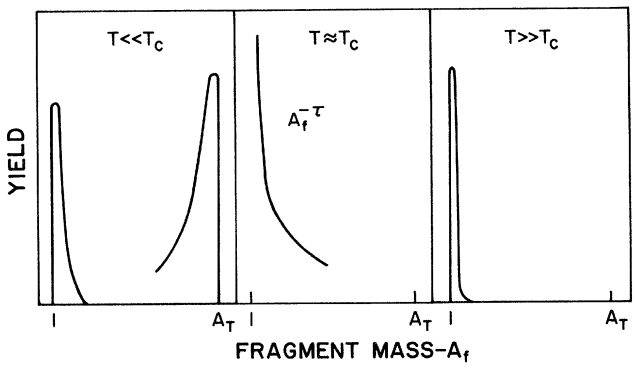

FIG. 15. Mass yield vs A_f for three temperature regimes of the remnant A_R. Power law behavior according to Eq. (1) is obtained only when the remnant temperature T is near T_c and $\rho \sim \rho_c$.

celerator Division, the Internal Target Group, and the PREP Group at Fermilab. We express our gratitude especially to F. R. Huson, R. Mau, P. McIntyre, D. Mizicko, and C. Nila. The assistance of S. Agarwal, J. T. Chuang, R. J. De Bonte, R. Forster, G. Paderewski, and Yu-Wen Yu was much appreciated. This work was supported by the U. S. Department of Energy and the National Science Foundation.

---

*Present address: Applied Mathematics, 1616 Route 12, Box 373, Gales Ferry, CT 06335.

†Present address: Lawrence Livermore Laboratory, Livermore, CA 94550.

[1]N. A. Perfilov, O. V. Lozhkin, and V. P. Shamov, Usp. Fiz. Nauk 60, 3 (1960) [Sov. Phys.—Usp. 3, 1 (1960)].

[2]J. Hudis, *Nuclear Chemistry,* edited by L. Yaffe (Academic, New York, 1968), Vol. 1, Chap. 3.

[3]R. Wolfgang, E. W. Baker, A. A. Caretto, J. B. Cumming, G. Friedlander, and J. Hudis, Phys. Rev. 103, 394 (1956); O. Scheidemann and N. T. Porile, Phys. Rev. C 14, 1534 (1976).

[4]A. M. Poskanzer, G. W. Butler, and E. K. Hyde, Phys. Rev. C 3, 882 (1971).

[5]G. D. Westfall, R. W. Sextro, A. M. Poskanzer, A. Zebelman, G. W. Butler, and E. K. Hyde, Phys. Rev. C 17, 1368 (1978).

[6]J. A. Gaidos, L. J. Gutay, A. S. Hirsch, R. Mitchell, T. V. Ragland, R. P. Scharenberg, F. Turkot, R. B. Willmann, and C. L. Wilson, Phys. Rev. Lett. 42, 82 (1979).

[7]J. E. Finn, S. Agarwal, A. Bujak, J. Chuang, L. J. Gutay, A. S. Hirsch, R. W. Minich, N. T. Porile, R. P. Scharenberg, B. C. Stringfellow, and F. Turkot, Phys. Rev. Lett. 49, 1321 (1982).

[8]R. W. Minich, S. Agarwal, A. Bujak, J. Chuang, J. E. Finn, L. J. Gutay, A. S. Hirsch, N. T. Porile, R. P. Scharenberg, B. C. Stringfellow, and F. Turkot, Phys. Lett. 118B, 458 (1982).

[9]C. S. Kiang, Phys. Rev. Lett. 24, 47 (1970).

[10]M. E. Fisher, Physics (N.Y.) 3, 255 (1967); Rep. Prog. Phys. 30, 615 (1967).

[11]A. M. Zebelman, W. G. Meyer, K. Halbach, A. M. Poskanzer, R. G. Sextro, G. Gabor, and D. A. Landis, Nucl. Instrum. Methods 141, 443 (1977).

[12]M. Fowler and R. Jared, Nucl. Instrum. Methods 124, 341 (1975).

[13]D. M. Barrus and R. L. Black, Rev. Sci. Instrum. 48, 116 (1982).

[14]J. E. Finn, Ph.D. thesis, Purdue University, 1982 (unpublished).

[15]J. W. Tippie and J. E. Kuluga, IEEE Trans. Nucl. Sci. NS-24, No. 1 (1977), SNAP system for nuclear data acquisition and processing.

[16]V. D. Bartenev *et al.*, Phys. Rev. Lett. 31, 1088 (1973); D. Gross *et al.*, *ibid.* 41, 217 (1978).

[17]A. S. Hirsch (private communication).

[18]L. Meyer, Phys. Status Solidi (b) 44, 253 (1971).

[19]D. A. Eastham, Nucl. Instrum. Methods 178, 539 (1980).

[20]Y. P. Yakovlev, Fiz. Elem. Chastits At. Yadra 8, 255 (1977) [Sov. J. Part. Nucl. 8, 106 (1977)].

[21]A. I. Warwick *et al.*, Phys. Rev. C 27, 1083 (1983).

[22]H. H. Gutbrod, A. I. Warwick, and H. Weiman, Nucl. Phys. A387, 177 (1982).

[23]H. E. Stanley, *Phase Transitions and Critical Phenomena,* edited by W. Marshall and D. H. Wilkinson (Oxford University, New York, 1971).

[24]D. Stauffer, Phys. Rep. 54, 1 (1979).

[25]R. W. Minich, Ph.D. thesis, Purdue University, 1981 (unpublished).

[26]A. S. Goldhaber, Phys. Lett. 53B, 306 (1974); Phys. Rev. C 17, 2243 (1978).

[27]E. J. Moniz, I. Sick, R. R. Whitney, J. R. Ficenec, R. D. Kephart, and W. P. Trower, Phys. Rev. Lett. 26, 445 (1971).

[28]A. Z. Mekjian, Phys. Rev. C 17, 1051 (1978).

[29]D. G. Ravenhall, C. J. Pethick, and J. M. Lattimer, University of Illinois Report ILL-(TH)-82-42, 1982.

[30]M. W. Curtin, H. Toki, D. K. Scott, Phys. Lett. 123B, 289 (1983).

[31]H. Jaqaman, A. Z. Mekjian, and L. Zamick, Rutgers University Report No. RU-83-61, 1983.

[32]G. Sauer, H. Chandra, and U. Mosel, Nucl. Phys. A264, 221 (1976).

[33]B. Friedman and V. R. Pandharipande, Nucl. Phys. A361, 502 (1981).

[34]G. Ropke, L. Munchow, and H. Schulz, Phys. Lett. 110B, 21 (1982).

[35]M. Nagasaki, Prog. Theor. Phys. 29, 415 (1963).

[36]K. Nakai *et al.*, Phys. Lett. 121B, 373 (1983); T.-A. Shibata *et al.*, University of Tokyo Report UTPN-195, 1983.

[37]R. Kaczarowski and E. Makowska, Nucl. Phys. 74, 348 (1965).